Boundary-Layer Meteorol
DOI 10.1007/s10546-011-9660-y

ARTICLE

Monin–Obukhov Similarity Functions for the Structure Parameters of Temperature and Humidity

Dan Li · Elie Bou-Zeid · Henk A. R. De Bruin

Received: 15 February 2011 / Accepted: 27 September 2011

Abstract Monin–Obukhov similarity functions for the structure parameters of temperature and humidity are needed to derive surface heat and water vapour fluxes from scintillometer measurements and it is often assumed that the two functions are identical in the atmospheric surface layer. Nevertheless, this assumption has not yet been verified experimentally. This study investigates the dissimilarity between the turbulent transport of sensible heat and water vapour, with a specific focus on the difference between the Monin–Obukhov similarity functions for the structure parameters. Using two datasets collected over homogeneous surfaces where the surface sources of sensible heat and water vapour are well correlated, we observe that under stable and very unstable conditions, the two functions are similar. This similarity however breaks down under weakly unstable conditions; in that regime, the absolute values of the correlations between temperature and humidity are also observed to be low, most likely due to large-scale eddies that transport unsteadiness, advection or entrainment effects from the outer layer. We analyze and demonstrate how this reduction in the correlation leads to dissimilarity between the turbulent transport of these two scalars and the corresponding Monin–Obukhov similarity functions for their structure parameters. A model to derive sensible and latent heat fluxes from structure parameters without measuring the friction velocity is tested and found to work very well under moderately to strongly unstable conditions ($-z/L > 0.5$). Finally, we discuss the modelling of the cross-structure parameter over wet surfaces, which is crucial for correcting water vapour effects on optical scintillometer measurements and also for obtaining surface sensible and latent heat fluxes from the two-wavelength scintillometry.

D. Li (✉) · E. Bou-Zeid
Department of Civil and Environmental Engineering, Princeton University, Princeton, NJ 08544, USA
e-mail: danl@princeton.edu

H. A. R. De Bruin
Freelance Consultant, Bilthoven, The Netherlands

H. A. R. De Bruin
King's College, London, UK

Published online: 20 October 2011

Keywords Evaporation · Monin–Obukhov similarity · Scintillometry · Structure parameters · Temperature–humidity similarity

1 Introduction

Long term measurements of surface heat and water vapour fluxes over large-scale natural landscapes are critical for a better understanding of the regional and global energy and water cycles. Such measurements also play an important role in improving numerical weather prediction and climate models since they allow the development of better parametrizations for surface fluxes in these models, thus providing the required boundary conditions. Since the 1970s, scintillometers have been widely used for surface flux measurements over a wide range of surface conditions (Andreas 1989, 1990; De Bruin et al. 1993, 1995, 2002; Green et al. 2001; Hartogensis et al. 2002; Meijninger et al. 2002a,b, 2006; Hartogensis and De Bruin 2005; Beyrich and Mengelkamp 2006; Roth et al. 2006; Leijnse et al. 2007; Kleissl et al. 2008, 2009; Nadeau et al. 2009). Compared to traditional point measurements such as standard eddy-covariance measurements, scintillometers have the advantages of being able to measure the path-integrated surface fluxes of sensible heat, latent heat, and momentum over large-scale, heterogeneous surfaces without flow distortion effects. Particularly in the frequent non-stationary and shallow stable boundary layer, scintillometers are more capable of capturing surface fluxes because of their short averaging intervals and low measurement heights (De Bruin et al. 2002; Hartogensis et al. 2002; Hartogensis and De Bruin 2005).

According to the wavelength used, scintillometers are often divided into two types: optical scintillometer (usually emitting infrared light produced by light emitting diodes or red laser light) and microwave scintillometers. Optical scintillometers are primarily sensitive to temperature fluctuations while microwave scintillometers are sensitive to both temperature fluctuations and humidity fluctuations (Andreas 1989). Thus, optical scintillometers are usually used for measuring the sensible heat flux, while a combination of an optical scintillometer and a microwave scintillometer is needed for measuring the latent heat flux (Andreas 1989; Green et al. 2001; Meijninger et al. 2002a,b, 2006; Beyrich and Mengelkamp 2006).

The basic quantities that can be derived from scintillometer measurements are the structure parameters of temperature and humidity, C_T^2 and C_q^2, which we will define later in detail. To obtain surface fluxes, Monin–Obukhov similarity functions relating the fluxes to the structures parameters are then needed. It is often assumed that these Monin–Obukhov similarity functions, or the flux–structure parameter relationships, for temperature and humidity are identical; however, this assumption has not yet been verified experimentally. Non-local effects such as advection (Lee et al. 2004; Assouline et al. 2008), modulations from the outer layer including unsteadiness (McNaughton and Laubach 1998) and entrainment at the top of the atmospheric boundary layer (Mahrt 1991; Sempreviva and Hojstrup 1998; De Bruin et al. 1999; Sempreviva and Gryning 2000; Asanuma et al. 2007; Cava et al. 2008; Katul et al. 2008), and differences in sources and sinks (Moriwaki and Kanda 2006; Williams et al. 2007; Detto et al. 2008; Moene and Schuttemeyer 2008) are particularly known to result in a breakdown of the similarity between turbulent transports of temperature and humidity. Therefore, the existence of these non-local effects might lead to differences in the Monin–Obukhov similarity functions for the structure parameters of these two scalars.

Our study aims at analyzing the similarity between temperature and humidity, under idealized conditions where non-local effects are minimized, although we will later see that some of these effects are still present; we specifically focus on the difference in the flux–structure parameter relationships. The paper proceeds as follows: Sect. 2 briefly reviews the basic

theory of scintillometry, and Sect. 3 describes the experimental set-up and data processing. In Sect. 4, we determine experimentally and compare the Monin–Obukhov similarity functions for the structure parameters of temperature and humidity, then investigate and discuss the difference between the two functions in the broader context of dissimilarity between the turbulent transport of sensible heat and water vapour. A model for deriving surface heat and water vapour fluxes under unstable conditions from scintillometer measurements without measuring the friction velocity is derived and tested in Sect. 5. In Sect. 6, two approaches for modelling the cross-structure parameter C_{Tq} over wet surfaces are examined, and conclusions are presented in Sect. 7.

2 Theory

A scintillometer is composed of two parts: a transmitter and a receiver. The transmitter emits electromagnetic radiation of constant intensity. The variance of the logarithm of the intensity measured by the receiver is proportional to the structure parameter of the refractive index (Wang et al. 1978):

$$\left\langle C_n^2 \right\rangle = 4.48\sigma_{\ln\ A}^2 D^{7/3} L^{-3}, \tag{1}$$

where $\left\langle C_n^2 \right\rangle$ is the path-averaged structure parameter of the refractive index of the air, $\sigma_{\ln\ A}^2$ is the variance of the natural logarithm of the intensity A, D is the aperture diameter, and L is the path length or distance between the emitter and the receiver.

The structure parameter of the refractive index is related to the structure parameters of temperature (C_T^2), specific humidity (C_q^2) and the cross-structure parameter (C_{Tq}) through the following relationship (Hill et al. 1980; Moene et al. 2004):

$$C_n^2 = \frac{A_T^2}{\overline{T}^2} C_T^2 + \frac{2A_T A_q}{\overline{T}\,\overline{q}} C_{Tq} + \frac{A_q^2}{\overline{q}^2} C_q^2, \tag{2}$$

where A_T and A_q are constants depending on the wavelength λ (m), average temperature $\overline{T}$ (K), average specific humidity $\overline{q}$ (kg kg^{-1}), and average pressure $\overline{P}$ (N m^{-2}). Since the equation has three unknowns, C_T^2, C_{Tq} and C_q^2, a solution cannot be obtained unless more equations are introduced or assumptions are made. One way to solve for the three unknowns is to use three wavelengths, which is highly expensive and difficult to implement (Andreas 1990). For optical scintillometers, the small dependence of C_n^2 on C_{Tq} and C_q^2 is simply regarded as a correction and only the sensitivity to temperature fluctuations, that is the C_T^2 term, is retained. In this way, the structure parameter of temperature can be obtained using only one wavelength (Hill 1997; Moene et al. 2004). This one-wavelength approach yields estimates of the sensible heat flux; however, modelling the effects of water vapour on the structure parameter of the refractive index, mainly through the cross-structure parameter C_{Tq}, remains a challenge, particularly over wet surfaces (Moene 2003). The intermediate method, called the two-wavelength method, is to measure C_n^2 using two wavelengths (typically optical and microwave) while modelling one unknown, C_{Tq}, as a function of two other unknowns C_T^2 and C_q^2. This method has the advantage of providing both the sensible and latent heat fluxes and has been the subject of theoretical and experimental studies in the past decade (Andreas 1989; Green et al. 2001; Beyrich and Mengelkamp 2006; Meijninger et al. 2006). Once C_T^2 and C_q^2 are obtained from scintillometer measurements, Monin–Obukhov

similarity functions are employed to compute sensible and latent heat fluxes following:

$$\frac{(kz)^{2/3}\, C_T^2}{T_*^2} = f_T(z/L), \tag{3a}$$

$$\frac{(kz)^{2/3}\, C_q^2}{q_*^2} = f_q(z/L), \tag{3b}$$

where κ is the von Karman constant (0.4), and z is the measurement height. The surface-layer temperature and humidity scales, T_*, q_*, and the Obukhov length scale L are defined as:

$$T_* = -\frac{H}{\rho c_p u_*}, \tag{4}$$

$$q_* = -\frac{L_v E}{\rho L_v u_*}, \tag{5}$$

$$L = -\frac{\overline{T} u_*^3}{\kappa g \left(\overline{w'T'} + 0.61\overline{T}\,\overline{w'q'}\right)}, \tag{6}$$

where H and $L_v E$ are the surface sensible and latent heat fluxes (W m^{-2}), respectively, u_* is the friction velocity, and ρ, C_p and L_v are the air density, the air specific heat capacity at constant pressure, and the latent heat of vaporization of water, respectively, and g is the gravitational acceleration (9.81 m s^{-2}). The prime denotes the turbulent fluctuations while the overbar (or brackets) denotes the Reynolds average, while thereafter u, v, and w denote the streamwise, transverse, and vertical velocities, respectively.

Several empirical functions for both unstable and stable conditions have been proposed (Wyngaard et al. 1971; Andreas 1989; Thiermann and Grassl 1992; De Bruin et al. 1993; Hartogensis and De Bruin 2005); we consider the following

$$\frac{(kz)^{2/3}\, C_T^2}{T_*^2} = c_{T1} k^{2/3} \left(1 - c_{T2}\frac{z}{L}\right)^{-2/3}, \tag{7a}$$

$$\frac{(kz)^{2/3}\, C_q^2}{q_*^2} = c_{q1} k^{2/3} \left(1 - c_{q2}\frac{z}{L}\right)^{-2/3}, \tag{7b}$$

for unstable conditions with $z/L < 0$ and

$$\frac{(kz)^{2/3}\, C_T^2}{T_*^2} = c_{T1} k^{2/3} \left(1 + c_{T2}\left(\frac{z}{L}\right)^{2/3}\right), \tag{8a}$$

$$\frac{(kz)^{2/3}\, C_q^2}{q_*^2} = c_{q1} k^{2/3} \left(1 + c_{q2}\left(\frac{z}{L}\right)^{2/3}\right), \tag{8b}$$

for stable condition with $z/L > 0$.

It is often assumed that the Monin–Obukhov similarity function for the structure parameter of humidity is identical to that of temperature. Hill (1989) pointed out that, if the structure and cross-structure parameters of temperature, humidity and refractive index all follow Monin–Obukhov similarity theory (MOST), then the similarity functions for all the structure and cross-structure parameters must be the same and the correlation coefficient between temperature and humidity must be equal to 1 (perfectly correlated) or -1 (perfectly anti-correlated). He further pointed out that MOST is an over-idealization of the dynamics of the surface layer and its interaction with the underlying surface, implying that dissimilarity is to be expected.

Given the fact that dissimilar transports of temperature and humidity are well documented (Katul and Hsieh 1999; Assouline et al. 2008), a direct measurement of the similarity function for humidity, and comparison to the function for temperature, are needed. This practical aim motivates our study; however, we also consider the dissimilar transport of heat and humidity in the turbulent atmospheric boundary layer (ABL) more generally since it has relevance for many hydrological and meteorological applications. Another practical aim related to scintillometer measurements is to examine the modelling of the cross-structure parameter over wet surfaces, which remains a challenge.

3 Experimental Set-Up and Data Processing

Two eddy-covariance datasets collected over Lake Geneva in Switzerland during the summer and autumn of 2006 and over the extensive "Plaine-Morte" Glacier from January to April 2008 are utilized for this study. The lake dataset covers the unstable to slightly stable regime while the glacier dataset covers the moderately stable to very stable regime. Both datasets include 20 Hz measurements of wind velocity, air temperature and water vapour concentration at four heights above the surface obtained using four pairs of sonic anemometers (Campbell Scientific CSAT3) and open-path gas analyzers (LICOR-7500). For the lake dataset, the four heights are 1.65, 2.30, 2.95 and 3.60 m; for the glacier dataset, the measurement heights change due to the accumulation of snow on the surface, with the average heights being 0.90, 1.90, 2.90 and 3.90 m. For the lake dataset, air density is calculated based on the air temperature measured by a Rotronic HygroClip S3 thermistor at 3.05 m and LICOR-measured pressure and water vapour concentration; then the specific humidity is computed from water vapour concentration and air density. Sonic-measured temperature is corrected for the effect of humidity to obtain air temperature at each height. For the glacier dataset, air density and specific humidity are calculated based on the sonic-measured temperature, LICOR-measured water vapour concentration and pressure, and the sonic-measured temperature is also corrected to obtain air temperature. We iterated the above procedure until the calculated air temperature converges but the resulting effect on air density and thus specific humidity is small. Other measurements include surface temperature and net radiation. Detailed description of the lake dataset (from the Lake-Atmosphere Turbulent EXchanges, LATEX, experiment) can be found in Bou-Zeid et al. (2008) and Vercauteren et al. (2008). The glacier dataset is presented in Huwald et al. (2009).

The Reynolds-averaging time chosen for this study is 15 min, though we also tested 30-min averaging but the results, as expected, did not change significantly. Data pre-processing mainly involves yaw and pitch correction, linear detrending and the density correction. In this study, data were also screened to ensure they obey the following criteria:

(1) The turbulence intensity must be less than 0.5 to justify the use of Taylor's hypothesis
(2) The standard deviations of velocity, temperature, water vapour concentration for each 15-min record must be five times larger than the root-mean-square (r.m.s.) noise of the instruments specified in the manuals, to ensure that the signal-to-noise ratio is sufficiently high
(3) The momentum and scalar fluxes must be larger than a threshold: $u_* > 0.01\,\mathrm{m\,s^{-1}}$, $|H| > 5\,\mathrm{W\,m^{-2}}$ and $|L_v E| > 5\,\mathrm{W\,m^{-2}}$, again to ensure the fluxes are well resolved by the instruments.

In addition, only flow from directions facing the sonic tower and flowing over a large upwind fetch of water or snow (on the order of 10 km for the lake and 1.5 km for the glacier)

are used, as in Vercauteren et al. (2008) and Bou-Zeid et al. (2010). The fetch-to-height ratios are thus larger than 2000:1 for the lake and 400:1 for the glacier. Surface sensible and latent heat fluxes H and L_vE, and friction velocities u_* are approximated by the measured turbulent fluxes that are calculated using the eddy-covariance method, following:

$$u_* = \left(\overline{u'w'}^2 + \overline{v'w'}^2\right)^{1/4}, \tag{9}$$

$$H = \rho C_p \overline{w'T'}, \tag{10}$$

$$L_vE = \rho L_v \overline{w'q'}. \tag{11}$$

The surface-layer temperature and humidity scales, T_* and q_*, are then calculated from Eqs. 4 and 5, respectively, and the Obukhov length scale, L, is computed from Eq. 6.

Based on Taylor's hypothesis, C_T^2 and C_q^2 are calculated from:

$$C_T^2 = \frac{D_T^2}{r^{2/3}} = \frac{\overline{[T(x) - T(x+r)]^2}}{r^{2/3}} = \frac{\overline{[T(x) - T(x+r)]^2}}{(\overline{u}\Delta t)^{2/3}}, \tag{12}$$

$$C_q^2 = \frac{D_q^2}{r^{2/3}} = \frac{\overline{[q(x) - q(x+r)]^2}}{r^{2/3}} = \frac{\overline{[q(x) - q(x+r)]^2}}{(\overline{u}\Delta t)^{2/3}}, \tag{13}$$

where D_T^2 and D_q^2 are the structure functions for temperature and humidity, $T(x)$ and $T(x+r)$ are air temperatures at location x and $x+r$, $q(x)$ and $q(x+r)$ are the specific humidities at location x and $x+r$, $\overline{u}$ is the average streamwise velocity, Δt is the translation time, and r is the translation distance that should lie within the inertial subrange. To ensure this constraint on r, we chose $r = z/2$ following Katul et al. (1997). We also tested whether this choice yields a value of r that is in, or at least close to, the inertial subrange; for example, we observed that the structure parameters vary as $r^{2/3}$. We note however that ensuring that all the statistics at scale r have inertial subrange scaling is virtually impossible (see for example Chamecki and Dias 2004); and departure from truly homogeneous isotropic turbulence is expected.

4 Results and Discussions

4.1 Similarity Functions for the Structure Parameters of Temperature and Humidity

Figure 1 shows our data for the variation of the normalized C_T^2 and C_q^2 under unstable conditions as a function of $-z/L$, and the functions fitted to our data using a non-linear least-squares method. The similarity functions proposed by Wyngaard et al. (1971) and De Bruin et al. (1993) are also shown for comparison. The similarity functions fitted to our data for non-dimensional C_T^2 and C_q^2 are:

$$\frac{(kz)^{2/3} C_T^2}{T_*^2} = 6.7k^{2/3}\left(1 - 14.9\frac{z}{L}\right)^{-2/3}, \tag{14}$$

$$\frac{(kz)^{2/3} C_q^2}{q_*^2} = 3.5k^{2/3}\left(1 - 4.5\frac{z}{L}\right)^{-2/3}. \tag{15}$$

Note that we fit our data by adopting the functional form proposed by Wyngaard et al. (1971) because of its simplicity and its ability to capture the variation of the data. Nevertheless, functions with higher powers of z/L were also proposed, for example by Thiermann and

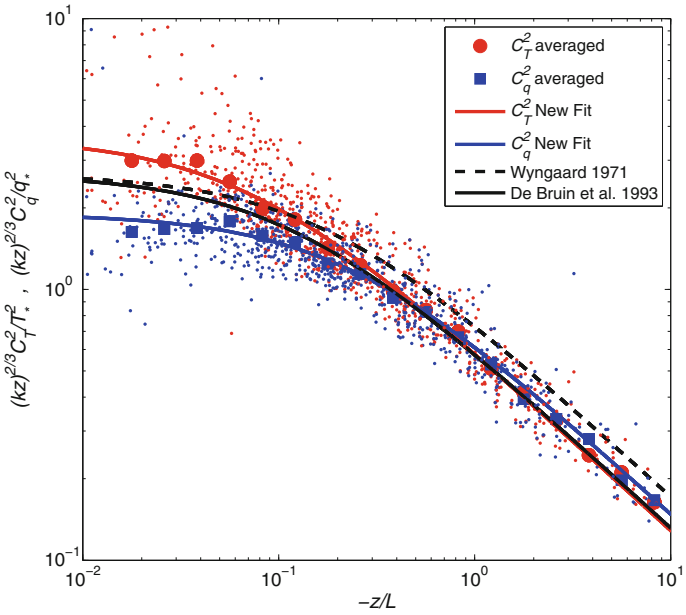

Fig. 1 Monin–Obukhov similarity functions for the structure parameters of temperature and humidity under unstable conditions. The small data points are from individual 15-min records, the large data points are bin averages over ranges of stabilities. Only the lake dataset is used

Grassl (1992). As shown in Fig. 1, the similarity functions for temperature and humidity are different under slightly unstable and near-neutral conditions ($0.01 < -z/L < 0.1$). As instability increases, the difference between the two functions gradually diminishes, implying that the transports of temperature and humidity become similar.

Figure 2 is also a fitting of MOST functions to our data for both C_T^2 and C_q^2 but under stable conditions; the relations shown in the figure are:

$$\frac{(kz)^{2/3}\,C_T^2}{T_*^2} = 4.5k^{2/3}\left(1 + 1.3\left(\frac{z}{L}\right)^{2/3}\right), \tag{16}$$

$$\frac{(kz)^{2/3}\,C_q^2}{q_*^2} = 3.5k^{2/3}\left(1 + 2.7\left(\frac{z}{L}\right)^{2/3}\right). \tag{17}$$

Under stable conditions, the Monin–Obukhov similarity function for the structure parameter of humidity is very close to that of temperature, due to the fact that temperature and humidity are highly correlated under these regimes, as will be discussed later. We point out that under very stable conditions, these similarity functions could in fact reflect local scaling rather than surface-layer MOST scaling since all the structure parameters are normalized by turbulent fluxes measured at the same height. However, since we do not study the variation of fluxes with height in detail here, we will still refer these as Monin–Obukhov similarity functions to be consistent with unstable and slightly stable conditions.

We compared our similarity functions for the structure parameter of temperature to previous studies that used the same functional forms indicated in Eqs. 7a and 8a. First note that, under convective conditions, the value of $c_{T1}c_{T2}^{-2/3}$ should be compared since it is this parameter that determines the shape of the function, while under weakly unstable conditions,

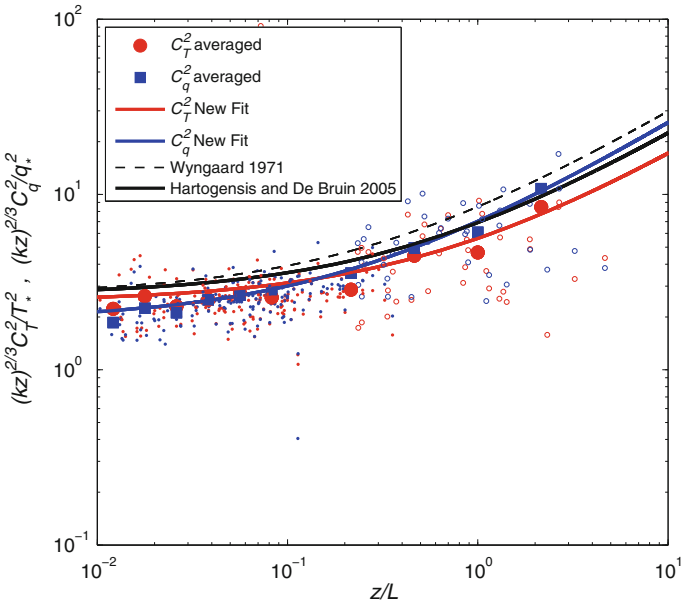

Fig. 2 Monin–Obukhov similarity functions for the structure parameters of temperature and humidity under stable conditions. The small data points are from individual 15-min records, the large data points are bin averages over ranges of stabilities. Both the lake (*solid dots*) and the glacier (*open circles*) datasets are used

Table 1 Similarity function coefficients for the structure parameter

	Unstable conditions			Stable conditions	
	c_{T1}	c_{T2}	$c_{T1}c_{T2}^{-2/3}$	c_{T1}	c_{T2}
Wyngaard et al. (1971)	4.9	6.1	1.47	4.9	2.2
Kohsiek (1982)			1.32		
De Bruin et al. (1993)	4.9	9	1.13	5.0	0
Hartogensis and De Bruin				4.9	1.6
This study (T) (95% confidence level)	6.7 ± 0.6	14.9 ± 4.0	1.11 ± 0.24	4.5 ± 0.7	1.3 ± 0.5
This study (q) (95% confidence level)	3.5 ± 0.1	4.5 ± 0.6	1.28 ± 0.14	3.5 ± 0.4	2.7 ± 0.5

the value of c_{T1} dominates. As shown in Table 1, our fitting functions differ to some extent from the previous functions proposed by Wyngaard et al. (1971) and De Bruin et al. (1993), but Fig. 1 illustrates that these two similarity functions are also within the ranges of our data scatter. Good agreement between different similarity functions under convective conditions is observed, with the coefficients $c_{T1}c_{T2}^{-2/3}$ we computed being very close to those reported in previous studies especially in De Bruin et al. (1993). It should be pointed out that the value of c_{T2} reported in Wyngaard et al. (1971) was modified by Andreas (1988) to account for the modification of κ from 0.35 to 0.4. The same modification was also applied here to the value of $c_{T1}c_{T2}^{-2/3}$ by Kohsiek (1982), which now becomes 1.32.

However, more significant differences between our similarity functions and those previously published are observed under stable conditions, which indicate larger uncertainties

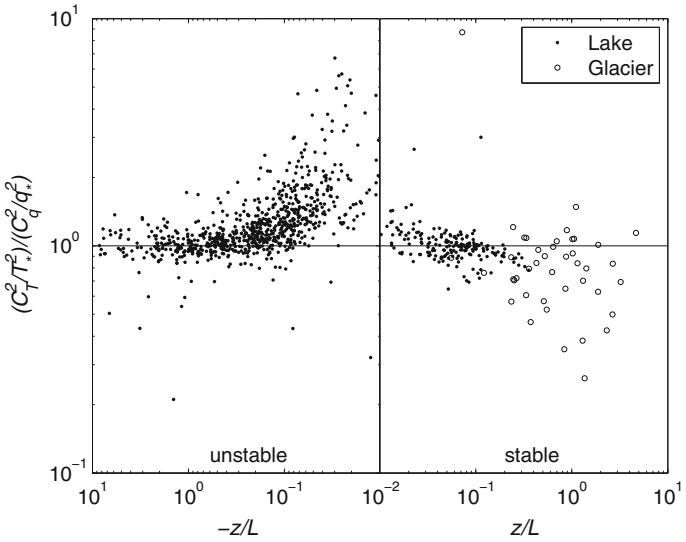

Fig. 3 The ratio of the normalized structure parameters of temperature and humidity

associated with Monin–Obukhov similarity functions of structure parameters compared to those in unstable conditions. For example, De Bruin et al. (1993) reported that the structure parameter of temperature under stable conditions, with large scatter, was almost constant at 5. The large scatter in Monin–Obukhov similarity functions under stable conditions could be associated with the intermittent nature of turbulence, the non-existence of a surface layer, large measurement errors in fluxes Mahrt (1999), or simply the inadequacy of flux-based stability parameters in capturing the physics of turbulence under stable conditions as outlined in Bou-Zeid et al. (2010), who showed that gradient-based parameters are better suited for stable conditions.

4.2 Dissimilarity of Turbulent Transport of Temperature and Humidity

As shown in Fig. 1, we observed differences in the similarity functions for the structure parameters of temperature and humidity under weakly unstable conditions ($-z/L < 0.1$). The parameters c_{T1} and c_{q1}, which determine the shape of the functions in this regime, are statistically different with no overlap in their 95% confidence bounds (i.e. the probability that their means are actually different despite the scatter is over 95%). It can be seen from Fig. 3 that the ratio of the normalized structure parameters of temperature and humidity becomes increasingly larger than unity as the instability decreases. Under convective conditions, the value of $c_{q1}c_{q2}^{-2/3}$ in our study is very close to that of $c_{T1}c_{T2}^{-2/3}$, implying that the two functions are very similar as illustrated in Fig. 3. The value of $c_{q1}c_{q2}^{-2/3}$ in Kohsiek (1982) after modification is 1.11 and is also very close to the value we obtained.

The dissimilarity between temperature and humidity is further investigated by using the correlation coefficient R_{Tq} since it is a good indicator of whether sensible heat and water vapour are transported similarly (De Bruin et al. 1999). In this study, the correlation coefficient R_{Tq} is calculated for each 15-min interval at each measurement height. A strong correlation (or anti-correlation) implies that the spatial distributions of the two parameters are similar (or exactly inverse) to each other and that the same eddies perform the transport

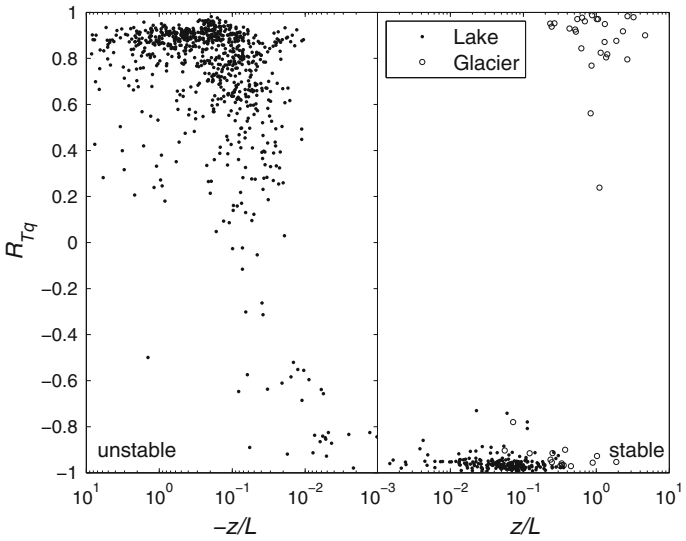

Fig. 4 Correlation coefficients for temperature and humidity

of both (in opposite directions if it is an anti-correlation). Under such conditions, even if the role of temperature as an active scalar is considerable, the resulting effects such as changes in transport efficiency (Li and Bou-Zeid 2011) will affect both scalars similarly. Due to the fact that the lake surface continuously evaporates, the sign of the correlation coefficient R_{Tq} depends on the direction of the sensible heat flux. Under unstable conditions, when sensible heat is transported upwards, R_{Tq} is positive, while under neutral and stable conditions, when sensible heat is transported downwards, R_{Tq} is negative. Note that, when $-z/L$ approaches zero from the unstable side (buoyancy is about zero, thus sensible heat flux has to be negative), the correlation coefficient decreases and becomes negative. However, for the glacier surface sensible heat is always transported downwards, and thus the sign of the correlation coefficient R_{Tq} depends on the direction of the latent heat flux. Under weakly stable conditions, the surface is still evaporating so the correlation coefficient R_{Tq} is negative. But as the stability increases, condensation commences and thus the correlation coefficient R_{Tq} turns positive.

As can be seen from Fig. 4, the absolute values of the correlation coefficient R_{Tq} are close to 1 under stable ($z/L > 0.01$) and neutral ($|z/L| < 0.01$) conditions, which agrees with Dias and Brutsaert (1996) and implies that sensible heat and water vapour are transported similarly. However, in unstable conditions, the correlation coefficient R_{Tq} behaves differently under different instabilities: under moderately to strongly unstable conditions ($-z/L > 0.5$), the correlation coefficients are high (around 0.9) with little scatter; when $0.1 < -z/L < 0.5$, there is some scatter associated with R_{Tq} but the values are still generally high (around 0.7); under weakly unstable conditions ($0.01 < -z/L < 0.1$), R_{Tq} decreases sharply and large scatter is observed in this regime. This de-correlation coincides with the difference in the Monin–Obukhov similarity functions for the structure parameters of temperature and humidity (Fig. 3).

Starting with the full transport equations of sensible heat and water vapour and using typical parametrizations and assumptions, the relationship between the ratio of the two similarity functions and the correlation coefficient R_{Tq} can be investigated theoretically, as shown in

Appendix A, and a general form can be obtained. When the dissimilarities in the flux–profile relationships, flux–variance relationships, and pressure transport terms of temperature and humidity are neglected (see Appendix A for analysis supporting these assumptions), but the dissimilarity in the buoyant production terms (which is related to the active role of temperature) is retained, the general relationship simplifies to the following analytical expression under unstable conditions:

$$\left(\frac{C_T^2}{T_*^2}/\frac{C_q^2}{q_*^2}\right)^{1/2} = \frac{A_T + B_T + C_T}{A_T + B_T + C_T R_{Tq}} = \frac{(A_T + B_T)/C_T + 1}{(A_T + B_T)/C_T + R_{Tq}}. \tag{18}$$

Note that A_T arises from the shear production term, B_T represents the pressure transport term and C_T represents the buoyant production term (see Appendix A for the expressions of these variables). It can be seen from Eq. 18 that the ratio of the two similarity functions depends on the correlation coefficient between the two scalars R_{Tq}. Consequently, similarities in flux–profile relationships and flux–variance relationships do not necessarily imply similarity in the flux–structure parameters relationships. The analytical expression in Eq. 18 shows that the ratio of the two similarity functions over the lake surface under unstable conditions is close to 1 when R_{Tq} is close to 1 and increases significantly as R_{Tq} decreases, regardless of the exact values of A_T, B_T and C_T, which are of the same order of magnitude based on a scaling analysis. As depicted in Fig. 5, the analytical model results with different values of A_T, B_T and C_T are consistent with the range of the measurements, which show the ratio is about 1 when R_{Tq} is high and becomes increasingly larger than 1 as R_{Tq} decreases.

The decorrelation between temperature and humidity over the lake surface under weakly unstable conditions, which results in dissimilarity in the flux–structure parameter relationships of the two scalars through the buoyancy production terms as illustrated above, is generally tied to non-local effects such as unsteadiness, advection, and entrainment in the outer layer, since the lake surface itself is the source for both temperature and humidity fluctua-

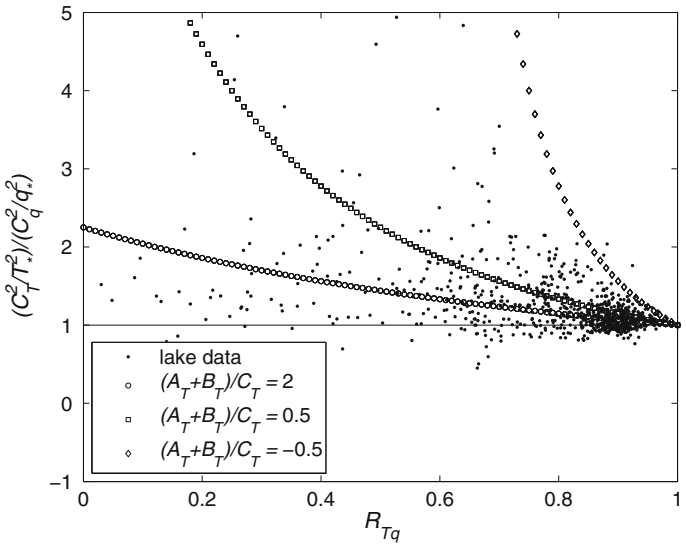

Fig. 5 The ratio of the flux–structure parameter relationships under unstable and evaporating surface conditions. The *circles*, *boxes*, and *diamonds* are model results, the *black dots* are measured data over the lake surface

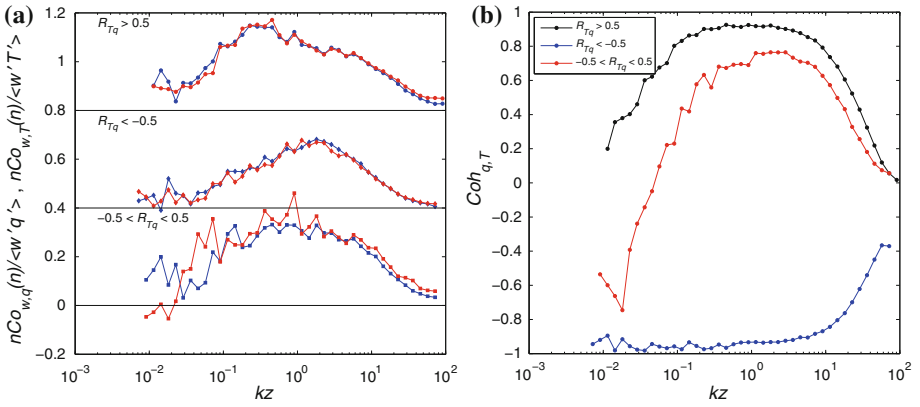

Fig. 6 Cospectra **a** and coherence spectra **b** of temperature and humidity in the three ranges of R_{Tq}. For illustration, the cospectra in the ranges of $R_{Tq} > 0.5$ and $R_{Tq} < -0.5$ are shifted up by 0.8 and 0.4, respectively, in (**a**); *blue lines* for q, *red* for T

tions, and is horizontally homogeneous over a fetch on the order of 10 km. When dry and hot air flows from the land to the lake surface, an internal boundary layer (IBL), whose depth is about 1/10 of the fetch (i.e. 1 km), will develop. Further down, an internal equilibrium layer (IEL), whose depth is about 1/10 of the IBL, that is, 100 m at our measurement location, will develop (Brutsaert 1998; Bou-Zeid et al. 2004). In the IEL, the micrometeorological variables are in dynamic equilibrium with the lake surface, thus the two scalars are transported similarly (Garratt 1990). Above the IEL, non-local effects, including advection, entrainment from the top of the ABL, or unsteadiness, prevail. Consequently, the dissimilarity between turbulent transport of temperature and humidity is likely to be related to the large-scale motions that transport these non-local effects from the outer layer to the surface layer and the IEL. This is further confirmed by the spectral analysis shown in Fig. 6. The whole dataset comprised 111 30-min runs that are separated into positive high correlation runs ($R_{Tq} > 0.5$, 70 runs), low correlation runs ($-0.5 < R_{Tq} < 0.5$, 16 runs), and negative high correlation runs ($R_{Tq} < -0.5$, 25 runs), respectively. Cospectra and coherence spectra are calculated for each full run (no binning) and then averaged over these three ranges of R_{Tq}.

From Fig. 6a we can see, when $R_{Tq} > 0.5$ or $R_{Tq} < -0.5$, the cospectra of temperature and humidity are very similar at all scales; however, when $-0.5 < R_{Tq} < 0.5$, the dissimilarity between temperature and humidity is manifest at large scales. In this low-correlation range, the very large-scale motions negatively contribute to the sensible heat flux (transporting high-temperature air downwards) but positively contribute to the water vapour flux (transporting high-water vapour concentration air upwards), which suggests that there is a layer of air with higher temperature aloft (either in the entrainment zone or at a lower height resulting from advection from the upstream land surface) acting as a source of sensible heat that the large-scale motions are transporting into the near-surface measurement zone. The dissimilarity in the dominant transport scales is also noticeable for the intermediate scales ($3 \times 10^{-2} < kz < 1$). The coherence spectra also show that the dissimilarity between temperature and humidity results from large-scale motions. It can be seen in Fig. 6b that, in the low-correlation range ($-0.5 < R_{Tq} < 0.5$), the coherence spectra between temperature and humidity at large scales are significantly lower in intensity than in the other two high-correlation ranges. A decrease in the coherence spectral intensities can also be noted for the

positive high correlation range ($R_{Tq} > 0.5$) when $kz = 2\pi z/l$ is below 0.1, i.e. when the scale $l > 200\,\mathrm{m}$, which roughly corresponds to our estimated IBL height.

McNaughton and Laubach (1998) studied how unsteadiness causes inequality in the turbulent diffusivities of temperature and humidity at the bottom of an internal boundary layer formed downwind of a dry-to-wet transition, similar to the lake site described in this study, except that the lake site has an even larger fetch-to-height ratio (2,000:1) than the 250:1 ratio reported in their study. Unsteadiness is also found in our study: turbulent fluxes computed for sub-intervals of the larger analysis intervals were sometimes different by up to 20% (not shown here). Dias et al. (2004) also studied several periods ranging from 1.5 to 3 h in length and reported that the decrease in the correlations R_{Tq} concurs with marked non-stationary effects that are reflected in the high values of the spectral densities of temperature fluctuations at low frequencies, which was also observed in previous studies (McNaughton and Laubach 2000; McNaughton and Brunet 2002). As a consequence, dissimilarity arises in the turbulent transport of temperature and humidity even close to the surface according to McNaughton and Laubach (1998). Advection or entrainment effects also reduce the correlation between temperature and humidity because hotter and dryer air from the upstream land or from the free atmosphere is now "sensed" by the instruments compared to hotter but wetter air from the surface. These also introduce fluctuations into the temperature field at large scales, which cascade down and lead to an increase in C_T^2 computed at scale r, but these fluctuations are not well correlated with vertical velocity fluctuations to produce or increase the surface flux H or T_*. The expected effect of this is to increase the value of C_T^2/T_*^2 relative to C_q^2/q_*^2, which is exactly what is observed in Fig. 1.

Asanuma et al. (2007) studied the correlation coefficients between temperature and humidity in the Fourier domain at scales similar to the height of the ABL and found that entrainment causes dissimilarity at such large scales. However, it is clear that these non-local effects extend to smaller scales only in the low-correlation range ($-0.5 < R_{Tq} < 0.5$), leading to a far lower correlation between temperature and humidity. The reason that the effects of these large-scale motions extend to the surface layer ($0.1 < kz < 5$) under weakly unstable conditions over the lake surface is that non-local effects now become significant compared to surface effects due to a reduced surface sensible heat flux. De Bruin et al. (1999) concluded that, if scalar fluxes are dominated by surface heating/evaporation, MOST and scalar similarity will hold; but if non-local effects are of equivalent importance to surface heating/evaporation, scalar similarity is likely to be violated (see also Mahrt 1991; McNaughton and Laubach 1998). Accordingly, under unstable conditions, MOST holds and the transport of two scalars are well-correlated. However, when the lower atmosphere is close to neutral, the surface sensible heat flux decreases and the non-local fluxes (i.e., entrainment fluxes or fluxes from the outer layer) become more significant in comparison, even though these fluxes in absolute terms may be lower than under convective conditions. The surface latent heat flux, on the other hand, is very strong and dominant over non-local effects under the same conditions, which explains why we still observe positive cospectra for humidity at large scales in Fig. 6a. We have further verified that this dissimilarity is not due to measurement errors related to small surface fluxes since we eliminated points where $H < 5\,\mathrm{W\,m^{-2}}$ to avoid such problems. However, when H is about 10 or $20\,\mathrm{W\,m^{-2}}$, the surface fluxes remain small and outer layer influences can be detected in our measurements. These weak heat-flux conditions do not occur in neutral conditions, naturally, but rather under slightly unstable conditions. Under neutral conditions ($|z/L| < 0.01$), the surface sensible heat flux is downwards, small but significant and is balanced, in the buoyancy flux term, by the upwards latent heat flux; the anti-correlated fluxes of heat and humidity at the surface under these conditions dominate the statistics at the measurement height and their similarity is restored.

The argument that non-local effects associated with large-scale motions result in decorrelation between temperature and humidity is consistent with previous studies that focus on the Bowen ratio (Lamaud and Irvine 2006; Moene and Schuttemeyer 2008) since the non-local effects become pronounced when one of the surface fluxes becomes smaller compared to the non-local fluxes, i.e. when the Bowen ratio is close to zero or very large. However, the occurrence of these non-local effects is different for the marine or lake boundary layer to that for the dry land boundary layer, as discussed in De Bruin et al. (1999). Over dry land surfaces, as the latent heat flux becomes smaller compared to the sensible heat flux or as the Bowen ratio increases, the correlation between temperature and humidity decreases. This typically occurs under unstable conditions (Mahrt 1991; De Bruin et al. 1993; Cava et al. 2008), while over water surfaces, as the atmosphere becomes neutral, the sensible heat flux becomes smaller compared to the latent heat flux. Thus, as the Bowen ratio decreases, we observe a decorrelation between temperature and humidity (Sempreviva and Hojstrup 1998; Sempreviva and Gryning 2000; Katul et al. 2008).

5 A Model for Surface Fluxes Under Convective Conditions

In this section, we use the two flux–structure parameter similarity functions for temperature and humidity to derive models for sensible and latent heat fluxes based on scintillometer measurements under sufficiently unstable conditions. Under such conditions, the unity in the parentheses in the flux–structure parameter relationships (Eqs. 14, 15) can be ignored, and the dependence of the fluxes on the friction velocity is eliminated (Kohsiek 1982). As mentioned before, the shapes of the flux–structure parameter relationships are determined by the values of $c_{T1}c_{T2}^{-2/3}$ and $c_{q1}c_{q2}^{-2/3}$ under unstable conditions; therefore, the calculations of sensible and latent heat fluxes should depend on these products. Furthermore, since the values of these products for temperature and humidity are very similar under moderately and strongly unstable conditions, we can neglect the small differences and use $c_{T1}c_{T2}^{-2/3} = c_{q1}c_{q2}^{-2/3} = 1.11$ (Table 1). This indicates that the calculations of the sensible and latent heat fluxes will only require a single Monin–Obukhov similarity function instead of two under such conditions. Then, by using the determined functional fit, the sensible and latent heat fluxes can be calculated from the following relationships:

$$\overline{w'T'} = \frac{0.58\left(C_T^2\left(\frac{g}{\overline{T}}\right)^{2/3} z^{4/3}\right)^{3/4}}{\left(1 + 0.61\overline{T}\sqrt{\frac{C_q^2}{C_T^2}}\right)}, \tag{19}$$

$$\overline{w'q'} = \sqrt{\frac{C_q^2}{C_T^2}} \times \overline{w'T'} = \sqrt{\frac{C_q^2}{C_T^2}} \frac{0.58\left(C_T^2\left(\frac{g}{\overline{T}}\right)^{2/3} z^{4/3}\right)^{3/4}}{\left(1 + 0.61\overline{T}\sqrt{\frac{C_q^2}{C_T^2}}\right)}. \tag{20}$$

These results are very useful for the combination of a large-aperture scintillometer with a microwave scintillometer since the large-aperture scintillometer cannot measure u_* directly, and thus requires either an independent measurement of u_* or an estimate of the wind velocity and of the surface roughness length z_0, which remains a highly challenging parameter to determine. With Eqs. 19 and 20, albeit only under sufficiently unstable conditions, the fluxes can be determined based only on the measurements provided by the two scintillometers and a mean temperature estimate (which has little effect on the calculations).

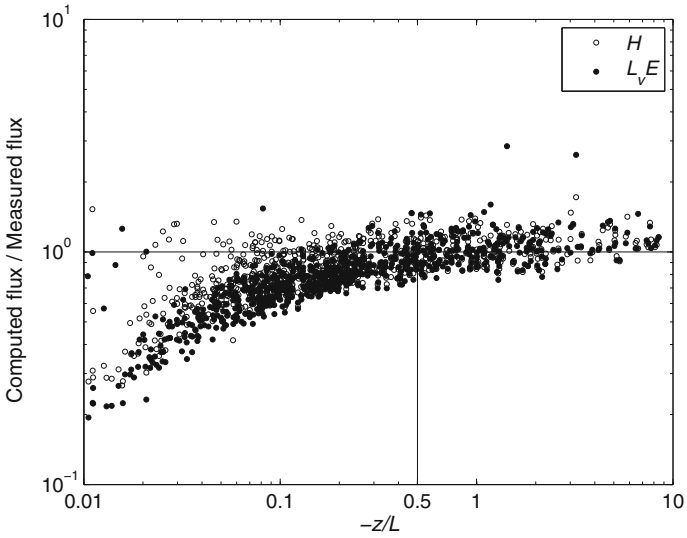

Fig. 7 The ratios of computed (Eqs. 19, 20) and measured sensible and latent heat fluxes.

These equations have been derived in previous studies (Kohsiek 1982; Meijninger et al. 2006); however, it is not clear yet at what value of $-z/L$ do these free-convection functions become applicable. Kohsiek (1982) observed the onset of the "free-convection limit" at $-z/L = 0.02$, noting that the relative errors for most of the surface sensible and latent heat fluxes calculated by these free-convection functions (Eqs. 19, 20) under $-z/L > 0.02$ are less than 30%. In this study, the ratios of computed sensible and latent heat fluxes based on Eqs. 19 and 20 to the measured sensible and latent heat fluxes, respectively, reached unity when $-z/L > 0.5$, as seen in Fig. 7. This is reasonable for sensible heat flux since as $-z/L$ approaches 0.5, the second term in the parentheses in the flux–structure parameter relationships ($c_{T2}z/L$) becomes almost an order of magnitude larger than unity, which justifies the elimination of the unity term in the parentheses of Eq. 14. For latent heat flux, it is slightly surprising because the value of $c_{q2}z/L$ is only 2.5. These results demonstrate the applicability of these free-convection functions at smaller values of $-z/L$ than we expected, though the value of 0.02 proposed by Kohsiek (1982) is not supported by our results.

6 The Cross-Structure Parameter C_{Tq}

The modelling of the cross-structure parameter is crucial for both optical scintillometers and the two-wavelength method. As mentioned before, for the two-wavelength method, C_{Tq} needs to be modelled as a function of C_T^2 and C_q^2 in order to solve the two equations with three unknowns; while for optical scintillometers used alone, the effects of water vapour on the structure parameter of refractive index are mainly through the cross-structure parameter C_{Tq}. For the two-wavelength method, C_{Tq} is usually modelled through

$$C_{Tq} = R_{Tq}\sqrt{C_T^2 C_q^2}, \tag{21}$$

where R_{Tq} is the correlation coefficient between humidity and temperature. It is often assumed that R_{Tq} is equal to unity but as pointed out by Ludi et al. (2005), a deviation

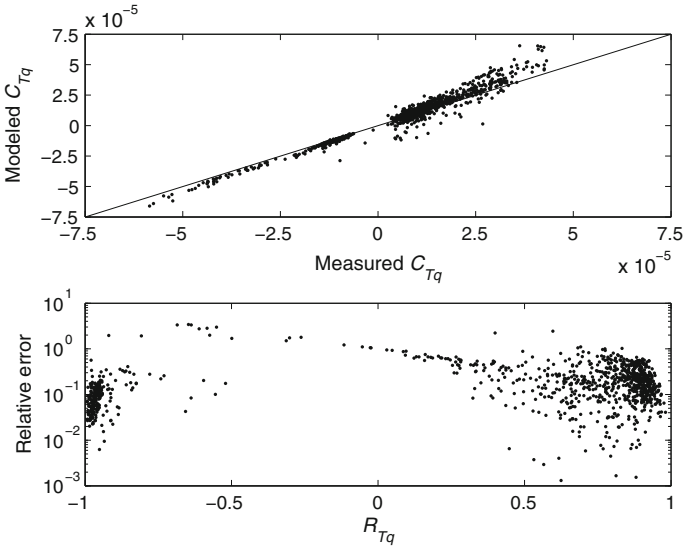

Fig. 8 Comparison between modelled (Eq. 21) and measured C_{Tq}

of R_{Tq} from unity leads to systematic errors in C_T^2 and C_q^2 estimates, especially for C_q^2. Kohsiek (1982) found that R_{Tq} calculated from Eq. 21 is approximately 0.75 and Ludi et al. (2005) also reported that assuming $R_{Tq} = 0.8$ would lead to better C_T^2 and C_q^2 estimates instead of assuming $R_{Tq} = 1$. For optical scintillometers, one way to model C_{Tq} is (Moene 2003):

$$C_{Tq} = C_T^2 R_{Tq}\,(0)\,\frac{\sigma_q}{\sigma_T}\left[\frac{1-\sqrt{R_{TT}\,(r)\,R_{qq}\,(r)}}{1-R_{TT}\,(r)}\right], \tag{22}$$

where $R_{TT}(r)$ and $R_{qq}(r)$ are autocorrelation functions of T and q at a separation distance r. Both of these methods, however, require additional measurements from a nearby eddy-covariance system (Meijninger et al. 2006; Leijnse et al. 2007). To overcome this problem, Ludi et al. (2005) developed a new method to estimate$C_{Tq}$from the correlation between the optical and microwave signals when the two-wavelength method is used, which was also successfully applied by Beyrich et al. (2005).

We revisit some of the assumptions involved in these approaches to compute C_{Tq} by testing the performance of Eqs. 21 and 22 over water surfaces. We compare modelled C_{Tq} from Eqs. 21 and 22 with measured values using the lake dataset, as shown in Figs. 8 and 9, respectively. In Fig. 8, general agreement is observed but discrepancy emerges when C_{Tq} is positive and large. This is further illustrated by the relative error between the modelled and measured C_{Tq}. The relative errors are higher when the absolute values of R_{Tq} are small; when R_{Tq} is close to -1, the relative errors are largely reduced, although it is surprising to notice that even when R_{Tq} is close to unity, the relative errors are still quite significant.

As seen from Fig. 9, it is clear that Eq. 22 does not perform better with even a larger relative error, especially when R_{Tq} values are close to unity. This is inconsistent with the results in Moene (2003), mainly because the dataset we used was collected over wet surfaces; thus the water vapour effects on the structure parameter of refractive index are expected to be more significant and different compared to dry land. We note that $R_{TT}(r)$ and $R_{qq}(r)$ are almost

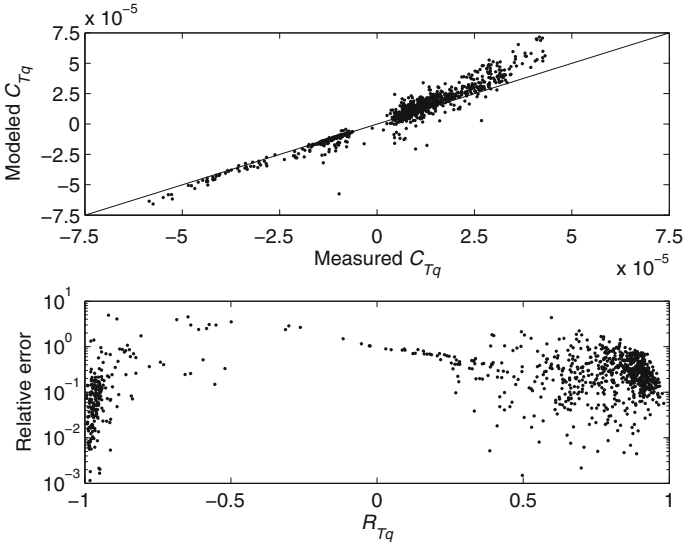

Fig. 9 Comparison between modelled (Eq. 22) and measured C_{Tq}

identical for the lake dataset, though. One implication of these comparisons for optical scintillometers and the two-wavelength scintillometry is that the modelling of the cross-structure parameter C_{Tq} over wet surfaces remains a challenging open research question.

7 Conclusions

The Monin–Obukhov similarity function for the structure parameter of humidity is often assumed to be identical to that for the structure parameter of temperature. This assumption is tested in study by direct measurements of the MOST flux–structure parameter relations for humidity under a very wide range of stabilities. It is found that the "best fits" of the similarity functions for temperature and humidity determined in this study are:

$$\frac{(kz)^{2/3}\,C_T^2}{T_*^2} = 6.7k^{2/3}\left(1 - 14.9\frac{z}{L}\right)^{-2/3}, \tag{23}$$

$$\frac{(kz)^{2/3}\,C_q^2}{q_*^2} = 3.5k^{2/3}\left(1 - 4.5\frac{z}{L}\right)^{-2/3}, \tag{24}$$

for unstable conditions ($z/L < 0$) and

$$\frac{(kz)^{2/3}\,C_T^2}{T_*^2} = 4.5k^{2/3}\left(1 + 1.3\left(\frac{z}{L}\right)^{2/3}\right), \tag{25}$$

$$\frac{(kz)^{2/3}\,C_q^2}{q_*^2} = 3.5k^{2/3}\left(1 + 2.7\left(\frac{z}{L}\right)^{2/3}\right), \tag{26}$$

for stable conditions ($z/L > 0$). For the temperature MOST relations, our fitting functions are close to previously proposed functions under unstable conditions, but they differ to some extent under stable conditions. From the fitting functions it is seen that the Monin–Obukhov

similarity function for the structure parameters of humidity is close to that for the structure parameters of temperature under all stable and most unstable conditions ($-z/L > 0.1$). However, under weakly unstable conditions ($0.01 < -z/L < 0.1$), statistically significant differences are observed between the two similarity functions. The difference in the two similarity functions for the structure parameters is investigated in the broader context of the dissimilarity between the turbulent transport of temperature and humidity. We propose a simple analytical model (Appendix A) that connects the difference in the two similarity functions to the dissimilarity in the flux–profile relationships, flux–variance relationships and also the correlation coefficients (R_{Tq}). It is found that, due to the high correlations of the two scalars, which implies that sensible heat and water vapour are transported similarly, the two flux–structure parameter relationships are similar under stable and most unstable conditions. However, R_{Tq} decreases sharply under weakly unstable conditions, which explains the large discrepancy between the two similarity functions in this regime. The reduced surface sensible heat fluxes in this regime reduces the importance of surface parameters, and allows large-scale processes that produce advection or entrainment effects from the outer layer or from outside the internal equilibrium layer to become important. This increase in the footprint of the outer layer then produces the decorrelation between temperature and humidity for the lake site.

Based on the MOST functions we compute here a simple model for deriving surface sensible heat and water vapour fluxes under convective conditions from scintillometer measurements, and which is independent of the friction velocity. It is found that the model provides very good estimates of these fluxes under moderately to strongly unstable conditions ($-z/L > 0.5$). Finally, two methods for modelling the cross-structure parameter, one for the two-wavelength method and the other for optical scintillometers, are tested over water surfaces. However, neither of them gives satisfactory results and the modelling of the cross-structure parameter over wet surfaces remains a challenging open research question.

Acknowledgment This work is supported by NSF under CBET-1058027 and by the Mid-Infrared Center For Health and the Environment at Princeton University. The authors would like to thank Professor Marc Parlange, Dr. Hendrik Huwald, Dr. Chad Higgins and the rest of the team of the Environmental Fluid Mechanics and Hydrology Laboratory at the Swiss Federal Institute of Technology—Lausanne where co-author Bou-Zeid was working during the two experiments described here, for the collection of the datasets. The authors would also like to thank Dr. Arnold Moene for his substantial suggestions, which helped improve the paper considerably.

Appendix A

The model presented here deals with dissimilarity between flux–structure parameter relationships over evaporating surfaces under unstable conditions. However, we are not constrained to the specific lake dataset that was used in this study. Our model relates the dissimilarity in flux–structure parameter relationships in a broad sense to the dissimilarity in flux–profile relationships, flux–variance relationships, and also to the correlation coefficient. Our aims are: first, to illustrate the potential causes for the dissimilarity in the flux–structure parameter relationships; second, to demonstrate that, even under conditions we encountered over the lake surface where the flux–profile relationships and the flux–variance relationships are identical for both scalars, a decorrelation of the two scalars results in difference in their flux–structure relationships.

Starting with the governing equations for heat and water vapour fluxes in a steady, horizontally homogeneous atmospheric surface layer with no subsidence and no significant flux-divergence (Katul and Hsieh 1999):

$$\frac{D\overline{w'T'}}{Dt} = 0 = -\overline{w'^2}\frac{\partial \overline{T}}{\partial z} + \frac{g}{\overline{T}}\overline{T'T'} - \frac{1}{\rho}\overline{T'\frac{\partial P'}{\partial z}} - 2\varepsilon_{wT}, \tag{27}$$

$$\frac{D\overline{w'q'}}{Dt} = 0 = -\overline{w'^2}\frac{\partial \overline{q}}{\partial z} + \frac{g}{\overline{T}}\overline{q'T'} - \frac{1}{\rho}\overline{q'\frac{\partial P'}{\partial z}} - 2\varepsilon_{wq}, \tag{28}$$

where D/Dt denotes the material derivative. In these equations we use the temperature but the derivation can easily be reproduced with the potential and virtual potential temperatures instead. The four terms on the right-hand-side (r.h.s.) of the two equations are: shear-production terms, buoyancy-production terms, pressure transport terms, and dissipation terms, respectively. The following Rotta-type parametrization for the pressure transport term for a generic scalar c (T or q) is then used (Moeng and Wyngaard 1986; Katul and Hsieh 1999):

$$\overline{c'\frac{\partial P'}{\partial z}} = \frac{c_{s,c}}{\tau}\overline{w'c'}, \tag{29}$$

where $c_{s,c}$ is a closure constant and τ is a characteristic time scale that depends on the turbulent kinetic energy (TKE) and the mean TKE dissipation rate (Katul and Hsieh 1999). We note that the dissipation term is zero if the flow and scalar field are locally isotropic. However, as summarized in Wyngaard (2010), shear flows with mean scalar gradients reach an equilibrium state of local anisotropy where this term is not zero. As such, the dissipation terms need to be estimated and here we will use the following parametrization proposed by Bradley et al. (1982):

$$\varepsilon_{wc} = a_1\left(\varepsilon\varepsilon_c\right)^{1/2}, \tag{30}$$

$$\varepsilon_c = \frac{C_c^2}{a_2}\varepsilon^{1/3}, \tag{31}$$

where ε is the dissipation rate of turbulent kinetic energy, ε_c is the dissipation rate of the variance of scalar c, and C_c^2 is the structure parameters of the scalar c. Also, a_1 and a_2 are positive constants, which we assume are identical for both temperature and humidity. While this assumption can be relaxed, this would complicate the analysis and is not deemed important: similarity for these parameters would be expected since they relate to viscous range dynamics that are not affected by dissimilarity at the large scales and where the active role of temperature is not significant.

Assuming steady-state conditions and substituting into the two flux-budget equations Eq. 27 and 28, yields:

$$0 = -\overline{w'^2}\frac{\partial \overline{T}}{\partial z} + \frac{g}{\overline{T}}\overline{T'T'} - \frac{1}{\rho}\frac{c_{s,T}}{\tau}\overline{w'T'} - 2a_1\left(\frac{C_T^2\varepsilon^{4/3}}{a_2}\right)^{1/2}, \tag{32}$$

$$0 = -\overline{w'^2}\frac{\partial \overline{q}}{\partial z} + \frac{g}{\overline{T}}\overline{q'T'} - \frac{1}{\rho}\frac{c_{s,q}}{\tau}\overline{w'q'} - 2a_1\left(\frac{C_q^2\varepsilon^{4/3}}{a_2}\right)^{1/2}. \tag{33}$$

We then invoke the following similarity functions (Stull 1988):

$$\frac{kz}{c_*}\frac{\partial \overline{c}}{\partial z} = \phi_c\left(\xi\right), \tag{34}$$

$$\frac{\sigma_c}{c_*} = \phi_{cc}\left(\xi\right), \tag{35}$$

where $\xi = z/L$. Substituting into Eqs. 32 and 33, and dividing by $|T_*|$ and $|q_*|$ respectively, we obtain:

$$2a_1 \frac{\varepsilon^{2/3}}{\sqrt{a_2}} \left(\frac{C_T^2}{T_*^2} \right)^{1/2} = \left(-\overline{w'^2} \frac{\phi_T}{kz} + \frac{1}{\rho} \frac{c_{s,T}}{\tau} u_* + \frac{g\sigma_T}{\overline{T}} \phi_{TT} \right) \frac{T_*}{|T_*|}, \tag{36}$$

$$2a_1 \frac{\varepsilon^{2/3}}{\sqrt{a_2}} \left(\frac{C_q^2}{q_*^2} \right)^{1/2} = \left(-\overline{w'^2} \frac{\phi_q}{kz} + \frac{1}{\rho} \frac{c_{s,q}}{\tau} u_* + \frac{g\sigma_T}{\overline{T}} \phi_{qq} R_{Tq} \right) \frac{q_*}{|q_*|}. \tag{37}$$

The correlation coefficient R_{Tq} stems from the buoyancy term in the water vapour flux budget equation. Dividing Eq. 36 by Eq. 37 yields:

$$\left(\frac{C_T^2}{T_*^2} \Big/ \frac{C_q^2}{q_*^2} \right)^{1/2} = \left(\frac{A_T + B_T + C_T}{A_q + B_q + C_q R_{Tq}} \right) \frac{T_*/|T_*|}{q_*/|q_*|}, \tag{38}$$

where

$$A_c = -\overline{w'^2} \frac{\phi_c}{kz}, \tag{39}$$

$$B_c = \frac{1}{\rho} \frac{c_{s,c}}{\tau} u_*, \tag{40}$$

$$C_c = \frac{g\sigma_T}{\overline{T}} \phi_{cc}. \tag{41}$$

We note that the left-hand sides of Eqs. 36 and 37 are positive, thus the r.h.s. must be positive, too. When $T_* < 0$ and $q_* < 0$, which corresponds to an evaporating surface and upward heat transfer (unstable conditions, which displayed the most dissimilarity in our data) with positive correlation between temperature and humidity, we must have:

$$(A_T + B_T + C_T) < 0, \tag{42a}$$

$$\left(A_q + B_q + C_q R_{Tq}\right) < 0. \tag{42b}$$

Equations 42 and the fact that R_{Tq} is positive for conditions when $T_* < 0$ and $q_* < 0$ imply that $R_{Tq} > \max\left(-\left(A_q + B_q\right)/C_q, 0\right)$. For the following analysis, we will be only focused on these conditions.

For simplicity, the similarity functions for humidity are expressed as the similarity functions for temperature multiplied by certain coefficients that reflect the dissimilarity in these similarity functions. Similarly, the coefficients in the pressure transport model (Eq. 40) are related in the same way:

$$\phi_q(\xi) = \alpha \phi_T(\xi) \tag{43a}$$

$$c_{s,q} = \gamma c_{s,T}. \tag{43b}$$

We also note the following exact relationship between the flux–variance relationships for temperature and humidity,

$$\phi_{qq}(\xi) = R_{wT}/R_{wq} \phi_{TT}(\xi), \tag{44}$$

Using Eqs. 43 and 44 and noting $T_* < 0$ and $q_* < 0$, Eq. 38 reduces to

$$\left(\frac{C_T^2}{T_*^2} \Big/ \frac{C_q^2}{q_*^2} \right)^{1/2} = \frac{A_T + B_T + C_T}{\alpha A_T + \gamma B_T + C_T \left(R_{wT}/R_{wq}\right) R_{Tq}}. \tag{45}$$

Computation of R_{wT}/R_{wq} from the lake data indicates that this ratio is very close to unity under all stability conditions (not shown here), implying similarity holds in the flux–variance relationships. It is also generally assumed that the normalized mean temperature and water vapour profiles, or the flux–profile relationships, are identical; that is, α in Eq. 45 is equal to 1 (e.g. Brutsaert 2005). Furthermore, we consider the case where the pressure transport is also similar and thus γ in Eq. 45 is also equal to 1; this reduces Eq. 45 to a model for cases where the dissimilarity between T and q results strictly from the buoyancy production terms (the second terms on the right in Eqs. 27 and 28), which is related to the active/buoyant role of temperature. Eq. 45 can otherwise still be used in its general form when detailed measurements allow all the terms to be quantified.

Hence, for this special case where dissimilarity mainly emanates from the buoyancy terms, and from the expression for C_T that indicates $C_T < 0$ and thus $C_T \leq C_T R_{Tq}$, we have

$$(A_T + B_T + C_T) \leq \left(A_T + B_T + C_T R_{Tq}\right). \tag{46}$$

Because the expressions on both sides of Eq. 46 are negative, this then yields the final results that we are seeking, viz.

$$\left(\frac{C_T^2}{T_*^2} \Big/ \frac{C_q^2}{q_*^2}\right)^{1/2} = \frac{A_T + B_T + C_T}{A_T + B_T + C_T R_{Tq}} \geq 1. \tag{47}$$

The physical implication of this result is that the active role of temperature, through the buoyancy production terms in the prognostic equations of the mean fluxes, results in a ratio of the normalized temperature structure parameter to the normalized humidity structure parameters that exceeds 1 whenever there is a decorrelation between the two scalars.

References

Andreas EL (1988) Atmospheric stability from scintillation measurements. Appl Opt 27(11):2241–2246

Andreas EL (1989) Two-wavelength method of measuring path-averaged turbulent surface heat fluxes. J Atmos Ocean Technol 6(2):280–292

Andreas EL (1990) Three-wavelength method of measuring path-averaged turbulent heat fluxes. J Atmos Ocean Technol 7(6):801–814

Asanuma J, Tamagawa I, Ishikawa H, Ma YM, Hayashi T, Qi YQ, Wang JM (2007) Spectral similarity between scalars at very low frequencies in the unstable atmospheric surface layer over the Tibetan plateau. Boundary-Layer Meteorol 122(1):85–103

Assouline S, Tyler SW, Tanny J, Cohen S, Bou-Zeid E, Parlange MB, Katul GG (2008) Evaporation from three water bodies of different sizes and climates: measurements and scaling analysis. Adv Water Resour 31(1):160–172

Beyrich F, Kouznetsov RD, Leps JP, Ludi A, Meijninger WML, Weisensee U (2005) Structure parameters for temperature and humidity from simultaneous eddy-covariance and scintillometer measurements. Meteorol Z 14(5):641–649

Beyrich F, Mengelkamp HT (2006) Evaporation over a heterogeneous land surface: EVA_GRIPS and the LITFASS-2003 experiment—an overview. Boundary-Layer Meteorol 121(1):5–32

Bou-Zeid E, Meneveau C, Parlange MB (2004) Large-eddy simulation of neutral atmospheric boundary layer flow over heterogeneous surfaces: Blending height and effective surface roughness. Water Resour Res 40(2):1–18

Bou-Zeid E, Vercauteren N, Parlange MB, Meneveau C (2008) Scale dependence of subgrid-scale model coefficients: an a priori study. Phys Fluids 20(11):115106-1–115106-6

Bou-Zeid E, Higgins C, Huwald H, Meneveau C, Parlange MB (2010) Field study of the dynamics and modelling of subgrid-scale turbulence in a stable atmospheric surface layer over a glacier. J Fluid Mech 665:480–515

Bradley EF, Antonia RA, Chambers AJ (1982) Streamwise heat-flux budget in the atmospheric surface-layer. Boundary-Layer Meteorol 23(1):3–15

Brutsaert W (1998) Land-surface water vapor and sensible heat flux: spatial variability, homogeneity, and measurement scales. Water Resour Res 34(10):2433–2442
Brutsaert W (2005) Hydrology: an introduction. Cambridge University Press, New York, 605 pp
Cava D, Katul GG, Sempreviva AM, Giostra U, Scrimieri A (2008) On the anomalous behaviour of scalar flux–variance similarity functions within the canopy sub-layer of a dense alpine forest. Boundary-Layer Meteorol 128(1):33–57
Chamecki M, Dias NL (2004) The local isotropy hypothesis and the turbulent kinetic energy dissipation rate in the atmospheric surface layer. Q J Roy Meteorol Soc 130(603):2733–2752
De Bruin HAR, Kohsiek W, Vandenhurk BJJM (1993) A verification of some methods to determine the fluxes of momentum, sensible heat, and water-vapor using standard-deviation and structure parameter of scalar meteorological quantities. Boundary-Layer Meteorol 63(3):231–257
De Bruin HAR, Van Den Hurk B, Kroon LJM (1999) On the temperature–humidity correlation and similarity. Boundary-Layer Meteorol 93(3):453–468
De Bruin HAR et al (1995) The scintillation method tested over a dry vineyard area. Boundary-Layer Meteorol 76(1–2):25–40
De Bruin HAR et al (2002) Displaced-beam small aperture scintillometer test. Part I: The WINTEX data-set. Boundary-Layer Meteorol 105(1):129–148
Detto M, Katul G, Mancini M, Montaldo N, Albertson JD (2008) Surface heterogeneity and its signature in higher-order scalar similarity relationships. Agric For Meteorol 148(6-7):902–916
Dias NL, Brutsaert W (1996) Similarity of scalars under stable conditions. Boundary-Layer Meteorology 80(4):355–373
Dias NL et al (2004) A study of spectra, structure and correlation functions and their implications for the stationarity of surface-layer turbulence. Boundary-Layer Meteorol 110(2):165–189
Garratt JR (1990) The internal boundary-layer—a review. Boundary-Layer Meteorol 50(1-4):171–203
Green AE, Astill MS, McAneney KJ, Nieveen JP (2001) Path-averaged surface fluxes determined from infrared and microwave scintillometers. Agric For Meteorol 109(3):233–247
Hartogensis OK, De Bruin HAR (2005) Monin–Obukhov similarity functions of the structure parameter of temperature and turbulent kinetic energy dissipation rate in the stable boundary layer. Boundary-Layer Meteorol 116(2):253–276
Hartogensis OK et al (2002) Displaced-beam small aperture scintillometer test. Part II: CASES-99 stable boundary-layer experiment. Boundary-Layer Meteorol 105(1):149–176
Hill RJ (1989) Implications of Monin–Obukhov similarity theory for scalar quantities. J Atmos Sci 46(14):2236–2244
Hill RJ (1997) Algorithms for obtaining atmospheric surface-layer fluxes from scintillation measurements. J Atmos Oceanic Technol 14(3):456–467
Hill RJ, Clifford SF, Lawrence RS (1980) Refractive-index and absorption fluctuations in the infrared caused by temperature, humidity, and pressure-fluctuations. J Opt Soc Am 70(10):1192–1205
Huwald H, Higgins CW, Boldi MO, Bou-Zeid E, Lehning M, Parlange MB (2009) Albedo effect on radiative errors in air temperature measurements. Water Resour Res 45:1–13
Katul G, Hsieh CI, Sigmon J (1997) Energy-inertial scale interactions for velocity and temperature in the unstable atmospheric surface layer. Boundary-Layer Meteorol 82(1):49–80
Katul GG, Hsieh CI (1999) A note on the flux–variance similarity relationships for heat and water vapour in the unstable atmospheric surface layer. Boundary-Layer Meteorology 90(2):327–338
Katul GG, Sempreviva AM, Cava D (2008) The temperature–humidity covariance in the marine surface layer: a one-dimensional analytical model. Boundary-Layer Meteorol 126(2):263–278
Kleissl J et al (2008) Large aperture scintillometer intercomparison study. Boundary-Layer Meteorol 128(1):133–150
Kleissl J et al (2009) Scintillometer intercomparison study—continued. Boundary-Layer Meteorol 130(3):437–443
Kohsiek W (1982) Measuring Ct2, Cq2, and Ctq in the unstable surface-layer, and relations to the vertical fluxes of heat and moisture. Boundary-Layer Meteorol 24(1):89–107
Lamaud E, Irvine M (2006) Temperature–humidity dissimilarity and heat-to-water-vapour transport efficiency above and within a pine forest canopy: the role of the Bowen ratio. Boundary-Layer Meteorol 120(1): 87–109
Lee X et al (2004) Micrometeorological fluxes under the influence of regional and local advection: a revisit. Agric For Meteorol 122(1–2):111–124
Leijnse H, Uijlenhoet R, Stricker JNM (2007) Hydrometeorological application of a microwave link: 1. Evaporation. Water Resour Res 43(4):W04416
Li D, Bou-Zeid E (2011) Coherent structures and the dissimilarity of turbulent transport of momentum and scalars in the unstable atmospheric surface layer. Boundary-Layer Meteorol 140(2):243–262

Ludi A, Beyrich F, Matzler C (2005) Determination of the turbulent temperature–humidity correlation from scintillometric measurements. Boundary-Layer Meteorol 117(3):525–550
Mahrt L (1991) Boundary-layer moisture regimes. Q J Roy Meteorol Soc 117(497):151–176
Mahrt L (1999) Stratified atmospheric boundary layers. Boundary-Layer Meteorol 90(3):375–396
McNaughton KG, Brunet Y (2002) Townsend's hypothesis, coherent structures and Monin-Obukhov similarity. Boundary-Layer Meteorol 102(2):161–175
McNaughton KG, Laubach J (1998) Unsteadiness as a cause of non-equality of eddy diffusivities for heat and vapour at the base of an advective inversion. Boundary-Layer Meteorol 88(3):479–504
McNaughton KG, Laubach J (2000) Power spectra and cospectra for wind and scalars in a disturbed surface layer at the base of an advective inversion. Boundary-Layer Meteorol 96(1–2):143–185
Meijninger WML, Beyrich F, Luedi A, Kohsiek W, De Bruin HAR (2006) Scintillometer-based turbulent fluxes of sensible and latent heat over a heterogeneous land surface—a contribution to LITFASS-2003. Boundary-Layer Meteorol 121(1):89–110
Meijninger WML, Green AE, Hartogensis OK, Kohsiek W, Hoedjes JCB, Zuurbier RM, De Bruin HAR (2002a) Determination of area-averaged water vapour fluxes with large aperture and radio wave scintillometers over a heterogeneous surface—Flevoland field experiment. Boundary-Layer Meteorol 105(1):63–83
Meijninger WML, Hartogensis OK, Kohsiek W, Hoedjes JCB, Zuurbier RM, De Bruin HAR (2002b) Determination of area-averaged sensible heat fluxes with a large aperture scintillometer over a heterogeneous surface—Flevoland field experiment. Boundary-Layer Meteorol 105(1):37–62
Moene AF (2003) Effects of water vapour on the structure parameter of the refractive index for near-infrared radiation. Boundary-Layer Meteorol 107(3):635–653
Moene AF, Meijninger, WML, Hartogensis OK, Kohsiek W, De Bruin HAR (2004) A review of the relationships describing the signal of a Large Aperture Scintillometer. Internal Report 2004/2. Meteorology and Air Quality Group, Wageningen University, Wageningen, the Netherlands, 40 pp
Moene AF, Schuttemeyer D (2008) The effect of surface heterogeneity on the temperature–humidity correlation and the relative transport efficiency. Boundary-Layer Meteorol 129(1):99–113
Moeng CH, Wyngaard JC (1986) An analysis of closures for pressure-scalar covariances in the convective boundary layer. J Atmos Sci 43(21):2499–2513
Moriwaki R, Kanda M (2006) Local and global similarity in turbulent transfer of heat, water vapour, and CO_2 in the dynamic convective sublayer over a suburban area. Boundary-Layer Meteorol 120(1):163–179
Nadeau DF et al (2009) Estimation of urban sensible heat flux using a dense wireless network of observations. Environ Fluid Mech 9(6):635–653
Sempreviva AM, Gryning SE (2000) Mixing height over water and its role on the correlation between temperature and humidity fluctuations in the unstable surface layer. Boundary-Layer Meteorol 97(2):273–291
Sempreviva AM, Hojstrup J (1998) Transport of temperature and humidity variance and covariance in the marine surface layer. Boundary-Layer Meteorol 87(2):233–253
Stull RB (1988) An introduction to boundary layer meteorology. Kluwer, Dordrecht, 670 pp
Thiermann V, Grassl H (1992) The measurement of turbulent surface-layer fluxes by use of bichromatic scintillation. Boundary-Layer Meteorology 58:367–389
Vercauteren N, Bou-Zeid E, Parlange MB, Lemmin U, Huwald H, Selker J, Meneveau C (2008) Subgrid-scale dynamics of water vapor, heat, and momentum over a lake. Boundary-Layer Meteorol 128(2):205–228
Wang TI, Ochs GR, Clifford SF (1978) Saturation-resistant optical scintillometer to measure C–N(2). J Opt Soc Am 68(3):334–338
Williams CA, Scanlon TM, Albertson JD (2007) Influence of surface heterogeneity on scalar dissimilarity in the roughness sublayer. Boundary-Layer Meteorol 122(1):149–165
Wyngaard JC (2010) Turbulence in the atmosphere. Cambridge University Press, Cambridge, New York, 393 pp
Wyngaard JC, Izumi Y, Collins SA (1971) Behavior of refractive-index-structure parameter near ground. J Opt Soc Am 61(12):1646